Solar Energy Materials & Solar Cells 157 (2016) 447–453

Contents lists available at ScienceDirect

Solar Energy Materials & Solar Cells

journal homepage: www.elsevier.com/locate/solmat

Enhanced short-circuit current density of perovskite solar cells using Zn-doped TiO_2 as electron transport layer

Ming-Chung Wu [a,b,c,*,1], Shun-Hsiang Chan [a,1], Meng-Huan Jao [d], Wei-Fang Su [d,**]

[a] Department of Chemical and Materials Engineering and Green Technology Research Center, Chang Gung University, Taoyuan 33302, Taiwan
[b] Center for Reliability Sciences & Technologies, Chang Gung University, Taoyuan 33302, Taiwan
[c] Division of Neonatology, Department of Pediatrics, Chang Gung Memorial Hospital, Taoyuan 33302, Taiwan
[d] Department of Materials Science and Engineering, National Taiwan University, Taipei 10617, Taiwan

ARTICLE INFO

Article history:
Received 21 December 2015
Received in revised form
27 May 2016
Accepted 3 July 2016
Available online 22 July 2016

Keywords:
Perovskite solar cell
Short-circuit current density
Zn-doped TiO_2
Electron transport layer
Charge carrier dynamics

ABSTRACT

In present work, we focused on the improvement of short-circuit current density (J_{sc}) by using zinc-doped TiO_2 (Zn-doped TiO_2) as electron transport layer. Various Zn-doped TiO_2 compact layers with different doping concentrations are prepared by sol-gel method followed thermal treatment, and they were then used to fabricate perovskite solar cell. Effects of zinc (Zn) on the power conversion efficiency (PCE), absorption behavior, crystal structure, electrical conductivity, and surface morphology are systemically elucidated. Charge carrier dynamics between perovskite active layer and titanium dioxide (TiO_2) compact layer is discussed too. When the dopant concentration is less than 5.0 mol%, the absorption behavior, electrical conductivity and charge separation efficiency increase with Zn doping concentration. In contrast, when the Zn dopant is 7.0 mol%, it results in the decay of these properties mentioned. According to the optimized processing of perovskite solar cells, the J_{sc} is increased from 18.5 to 22.3 mA/cm^2 so as to the PCE is significantly improved from 11.3% to 14.0%.

1. Introduction

Perovskite solar cells have attracted a great interest recently due to their potential application in developing low-cost, solution processable, large-area and mechanically flexible photovoltaic devices. In addition, perovskite solar cells show high power conversion efficiency (PCE), and the PCE have rapidly increased from 3.1% to 22.1% in only six years [1]. Many perovskite-type materials are usually used as the active layer for light harvesting because of their strong and broad light absorption characteristics in the visible range [2–7]. When it absorbs light energy larger than their bandgap, excitons are generated then they are immediately diffused and separated into electrons and holes. The electrons and the holes are injected to the electron transport layer and hole transport layer from perovskite layer respectively under the internal field built by n-i-p junction. If the charge carriers generated in the perovskite are not effectively transferred to the proper transport layers, they will be directly recombined, accumulated in the perovskite or interface, and the charge transport will be reduced [8–10].

For perovskite solar cells, many metal oxides, such as aluminum oxide (Al_2O_3) [11], zinc oxide (ZnO) [12], zirconium oxide (ZrO_2) [13], tin oxide (SnO_2) [7] and titanium dioxide (TiO_2) [14–18], have been applied to the electron transport layer for improving the PCE. Among these metal oxides, TiO_2 is a good candidate due to the chemical stability, low-cost, and high charge transport ability [19–21]. Moreover, the conduction band of TiO_2 is lower than the conduction band of perovskite active layer, so the electron can be effectively transported from perovskite active layer to TiO_2 compact layer [22]. However, there is a need to increase the conductivity of TiO_2 for efficient electron transport. Metal ion dopants in TiO_2 is a good subject to improve photocurrent and electron-hole recombination for perovskite solar cells. Niobium-doped TiO_2 (Nb-doped TiO_2) nanorod was adopted to enhance the charge transport for perovskite solar cells because it provides better conductivity and interface contact [23]. Yttrium-doped TiO_2 (Y-doped TiO_2) compact layer was used as the electron transport layer for n-i-p structure perovskite solar cell [24]. Magnesium-doped TiO_2 (Mg-doped TiO_2) compact layer exhibits higher photocurrent than pristine TiO_2 compact layer due to the improved band alignment between TiO_2 and perovskite [25]. Lithium-treated TiO_2 (Li-treated TiO_2) nanoparticle was inserted at the electron transport layer of perovskite solar cells, because lithium-treated

* Corresponding author at: Department of Chemical and Materials Engineering and Green Technology Research Center, Chang Gung University, Taoyuan 33302, Taiwan.
** Corresponding author.
E-mail addresses: mingchungwu@mail.cgu.edu.tw (M.-C. Wu), suwf@ntu.edu.tw (W.-F. Su).
[1] M.-C. Wu and S.-H. Chan contributed equally.

http://dx.doi.org/10.1016/j.solmat.2016.07.003
0927-0248/

Please cite this article as: M.-C. Wu, et al., Enhanced short-circuit current density of perovskite solar cells using Zn-doped TiO_2 as electron transport layer, Solar Energy Materials and Solar Cells (2016), http://dx.doi.org/10.1016/j.solmat.2016.07.003

TiO_2 had more favorable charge injection and better conductivity than pristine TiO_2 [26].

Zinc-doped TiO_2 (Zn-doped TiO_2) has drawn attention due to the low-cost of zinc (Zn) precursor and high electrical conductivity (i.e., low internal electrical resistance). It is indicated that Zn dopant is able to modify TiO_2 electronic structure [27–30]. Wang et al. added many metal precursors, including Y, Zr, molybdenum (Mo), and Zn compounds to interact with TiO_2 nanocrystals [31]. The results show that the Zn-doped TiO_2 exhibited the highest conductivity. Thus, the Zn dopant is expected to improve carrier transport and subsequently enhance the short-circuit current density (J_{sc}) of solar cell. Herein, we use Zn-doped TiO_2 compact layer as electron transport layer with different doping concentrations. Various n-i-p structure perovskite solar cells were fabricated. We also studied the crystal structure, absorption behavior, electrical conductivity and surface morphology of various Zn-doped TiO_2 compact layers. Furthermore, the correlation between the charge carrier dynamics and Zn doping concentration for various Zn-doped TiO_2 compact layers is explored by time-resolved photoluminescence (TRPL) measurements. The photovoltaic performances of perovskite solar cells with various Zn-doped TiO_2 compact layer as electron transport layer are reported. The results address the issues of improving the electron compact layer and thus helping the further design of highly efficient perovskite solar cells.

2. Experimental details

2.1. Materials and sample preparation

The methylammonium iodide (CH_3NH_3I, MAI) was synthesized similar to literature [32,33]. 30.0 mL hydriodic acid (HI, 57.0 wt% aqueous solution) was added into the methylamine (CH_3NH_2, 33.0 wt% in ethanol) with continuous stirring at 0 °C for 2 h under argon gas. The yellow solution was obtained and then rotary evaporated at 55 °C for 2 h to get the white precipitate. The white precipitate was purified in recrystallization with ethanol and diethyl ether. Finally, the pure MAI powder was dried at 60 °C in a vacuum oven for 24 h. The perovskite precursor solution (i.e., $CH_3NH_3PbI_{3-x}Cl_x$) was prepared by mixing MAI powder and lead chloride ($PbCl_2$, 99.999%) at 39.0 wt% in 1.0 mL dimethylformamide ($HCON(CH_3)_2$, DMF, anhydrous, 99.8%). In contrast, the 2,2',7,7'-Tetrakis [N,N-di(4-methoxyphenyl)amino]−9,9'-spirobifluorene (spiro-OMeTAD) solution was synthesized according to the literature [34]. 104 mg of lithium-bis-(trifluoromethanesulfonyl)imide (Li-TFSI, 99.95%) was dissolved in 200.0 μL acetonitrile (CH_3CN, 99.5%). The spiro-OMeTAD solution was well prepared by dissolving 80 mg spiro-OMeTAD, 28.5 μL 4-tert-butylpyridine (tBP, 96%), and 17.5 μL Li-TFSI solution in 1.0 mL chlorobenzene (C_6H_5Cl, CB, 99.8%) with continuous stirring. For the synthesis of TiO_2 precursor solution, 375 μL of titanium isopropoxide ($Ti(OCH(CH_3)_2)_4$, TTIP, >97%) was added to 2.5 mL of ethanol (C_2H_5OH, 99.5%). In a separate beaker, 35 μL of 2.0 M HCl solution was added to 2.5 mL of ethanol. It was then added to Ti precursor solution in continuous ice bath stirring. For Zn precursor solution, 26.4 mg of zinc nitrate hexahydrate ($Zn(NO_3)_2 \cdot 6H_2O$, >97%) was dissolved in 2.5 mL of ethanol until it was completely dissolved to form Zn precursor solution in vigorous stirring. Then, Zn precursor solution was added to Ti precursor solution with various stoichiometric ratio in continuous stirring for 2 h. All chemicals were purchased from commercial products without any purification.

2.2. Fabrication of the perovskite solar cells

The Zn-doped TiO_2 precursor solution was spin-coated on the FTO glass by 1000 rpm for 40 s and calcined at 550 °C for 30 min to form a Zn-doped TiO_2 compact layer. The FTO glass (7 Ω, Ruilong) was cleaned sequentially with detergent, methanol and isopropanol. The perovskite precursor solution was spin-coated on the Zn-doped TiO_2 compact layer by 2000 rpm for 45 s. Subsequently, the spiro-OMeTAD solution was spin-coated over a perovskite layer at 4000 rpm for 30 s. Finally, gold electrode was thermally deposited on the device surface through a shadow mask with 0.09 cm^2 active area. The performance of every perovskite solar cell was evaluated statistically by 12 separated solar cells in average.

2.3. Characterization

The current density-voltage (J-V) characteristic of the device was recorded by the source meter (Keithley 2410). Solar-simulated AM 1.5 sunlight was generated using an irradiation (Newport-69920, 100 mW/cm^2) calibrated with a silicon reference cell (Oriel P/N 91150V, VLSI standards) with KG-5 visible color filter. For the hysteresis measurement, the data is recorded under the reverse and forward bias in a 10 ms delay time. In forward bias, scanning has 5 s stabilization before illumination [35]. External quantum efficiency (EQE) was measured by IPCE spectrometer (EQE-R-3011, Enli Technology Co. Ltd). It was calibrated by a single-crystal silicon reference cell for each EQE measurements. Energy dispersive spectra (INCA Penta FET-x3, Oxford Instruments) was gathered in the field emission-SEM (JSM-7500 F, JEOL). The Zn-doped TiO_2 film was prepared for SEM/EDS measurement, and its film thickness is ~700 nm measured by alpha stepper (Dektak 6M Stylus Profilometer, Veeco). The accelerating voltage was set at 10 kV for Zn distinctive resolution of the prepared Zn-doped TiO_2 film. The detection time of each position were fixed at 200 s. X-ray photoelectron spectrometry (XPS, ULVAC-PHI Inc.) was used to analyze Zn doping concentration of various Zn-doped TiO_2 compact layers by using Al K_α radiation with a photoelectron 45° take off angle under high vacuum (~10^{-7} Torr). The surface morphology of various Zn-doped TiO_2 compact layers was observed by SEM (SNE-4500M, SEC) and AFM (Dimension-3100 Multimode, Digital Instruments) in tapping mode. UV–vis absorption spectra was measured by UV–vis spectrometer (V-630, Jasco). Synchrotron X-ray diffraction was performed by synchrotron X-ray spectroscopy (λ~1.025 Å) on beam line 13A1 of the National Synchrotron Radiation Research Center (NSRRC) in Taiwan. The steady state photoluminescence (PL) spectra were obtained by pumping the samples with a continuous-wave diode laser (λ_{exe}=440 nm, PDLH-440-25, DongWoo Optron Co. Ltd.). The emission spectra were analyzed by a photomultiplier tube detector system (PDS-1, DongWoo Optron Co. Ltd.) and standard photon-counting electronics using a monochromator (Monora 150i, DongWoo Optron Co. Ltd.). TRPL spectroscopy was performed using a time-correlated single photon counting (WELLS-001 FX, DongWoo Optron Co. Ltd.) spectrometer. A pulse laser (λ_{exe}=440 nm) with an average power of 1 mW, operating at 312.5 MHz, with 2 μs duration was used for excitation.

3. Results and discussion

Various Zn-doped TiO_2 compact layers exhibit the anatase phase as shown in Fig. 1(a). For the pristine TiO_2 compact layer, all diffraction peaks can be perfectly indexed as the body-centered tetragonal structure of TiO_2 anatase phase, with unit cell parameters a=b=3.78 Å and c=9.52 Å [COD ID:720675]. The intensity of (101) crystal plane for anatase TiO_2 phase decreases as the Zn doping concentration increases. However, the intensity of (110) crystal plane for rutile TiO_2 phase becomes obvious when the Zn doping concentration is above 3.0 mol%. The structural defects

Please cite this article as: M.-C. Wu, et al., Enhanced short-circuit current density of perovskite solar cells using Zn-doped TiO_2 as electron transport layer, Solar Energy Materials and Solar Cells (2016), http://dx.doi.org/10.1016/j.solmat.2016.07.003

introduced by the Zn ion can interacted with the surrounding anatase crystal, and Zn ion can activate the nucleation and growth of rutile TiO_2 phase [28]. In addition, XRD patterns show a slightly shift to smaller scattering angles due to the fact that the ionic radius of Zn^{2+} is large than Ti^{4+} (Fig. 1(b)) [29].

The absorption spectra of various Zn-doped TiO_2 compact layers show significantly red-shift as shown in Fig. 2(a). The bandgaps of pristine TiO_2 and 1.0, 3.0, 5.0 and 7.0 mol% Zn-doped TiO_2 compact layers are calculated from the UV–vis absorption spectra. Their values are 3.75, 3.73, 3.72, 3.58 and 3.26 eV, respectively (Fig. 2(b)). The bandgap of various Zn-doped TiO_2 compact layers is decreased with increasing Zn doping concentration for the presence of Zn ion introducing a new band within the TiO_2 bandgap. The previous reports indicated that Zn-doped TiO_2 compact layer could decrease the position of conduction band, so the lower conduction band can improve the electron injection from perovskite to Zn-doped TiO_2 compact layer [26,36,37]. In addition, the lower bandgap induced by the Zn doping concentration can be explained by the formation of lower bandgap rutile TiO_2 (3.03 eV) [38].

The zero-field vertical conductivities of various Zn-doped TiO_2 compact layers (i.e., concentration effect) were measured to obtain the correlation between electron transport behavior and Zn doping concentration. The current density-electric field (J-E) curves are shown in Fig. 3. The schematic diagram of the device for measuring the zero-field vertical conductivity is shown in the inset figure. The J-E curve was fitted by Poole-Frenkel model [39] as shown below:

$$J = \sigma_0 E \exp\left(\beta\sqrt{E}\right)$$

where σ_0 and β are the fitting parameter, σ_0 is the zero-field vertical conductivity and β is the Poole-Frenkel parameter. Electric field (E) was calculated from $E = V/L$, where L is the thickness of Zn-doped TiO_2 compact layer. In order to accurately calculate the voltage across the FTO/Zn-doped TiO_2/Au device, the voltage was calculated by $V = V_{applied} - J \cdot A \cdot r_{series}$. The r_{series} is 17 Ω for all of the sample and A is the active area (0.04 cm^2). Table 1 shows the conductivities of various Zn-doped TiO_2 compact layers. The conductivity substantially increases from 0.35 to 8.34 mS/m with increasing Zn doping concentration from 0.0 to 5.0 mol%. In contrast, the conductivity is 2.20 mS/m when Zn doping concentration is 7.0 mol%. It is possibly due to the formation of voids.

In order to investigate the surface morphologies of various Zn-doped TiO_2 compact layers, the samples are evaluated by SEM and AFM. The SEM images of various Zn-doped TiO_2 compact layers are shown in Fig. 4(a-e). The Zn-doped TiO_2 compact layer replicates remarkably well the underlying FTO relief morphology. The Zn-doped TiO_2 compact layers are uniform and continuous when the Zn doping concentration is less than 5.0 mol% as show in

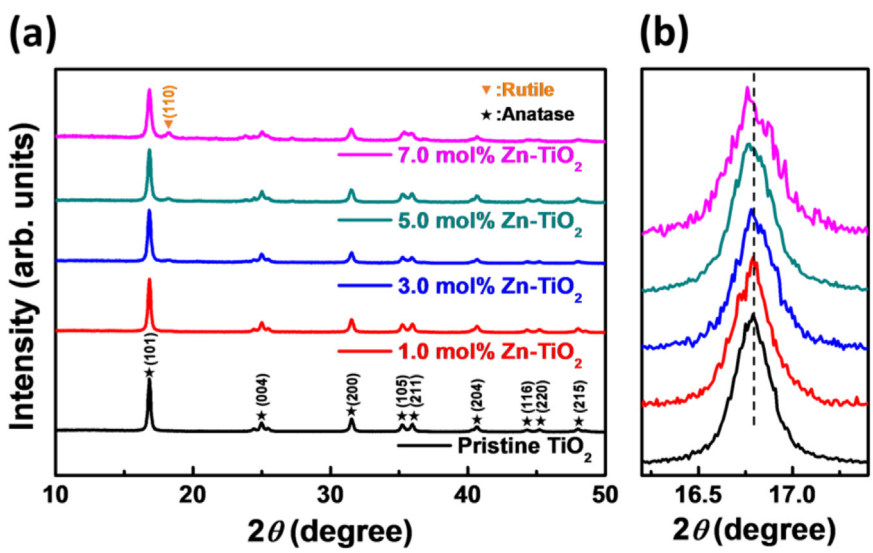

Fig. 1. Synchrotron X-ray spectra of (a) pristine TiO_2 and various Zn-doped TiO_2 and (b) magnified spectra.

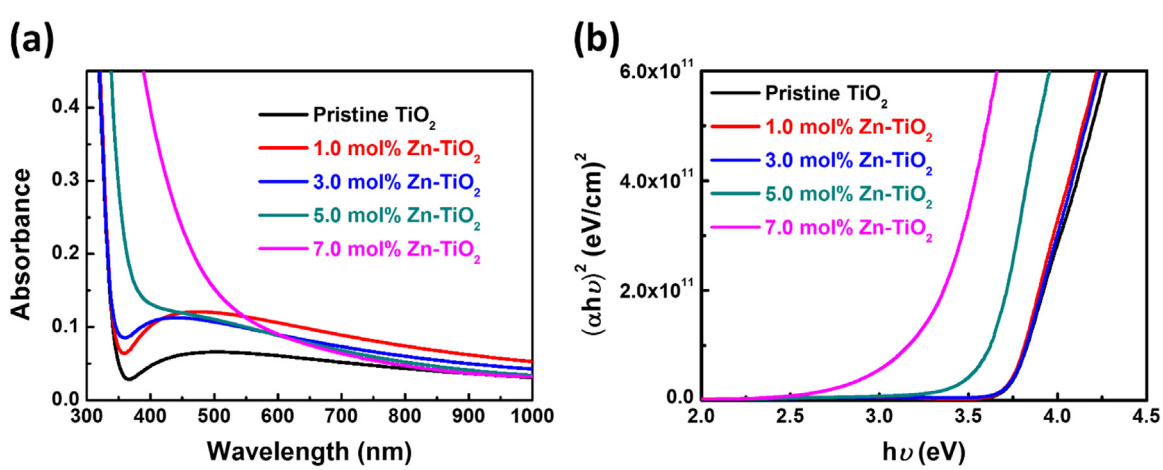

Fig. 2. (a) Absorption spectra and (b) the plot of $(\alpha h\nu)^2$ versus $h\nu$ of pristine TiO_2 and various Zn-doped TiO_2 compact layer.

Please cite this article as: M.-C. Wu, et al., Enhanced short-circuit current density of perovskite solar cells using Zn-doped TiO_2 as electron transport layer, Solar Energy Materials and Solar Cells (2016), http://dx.doi.org/10.1016/j.solmat.2016.07.003

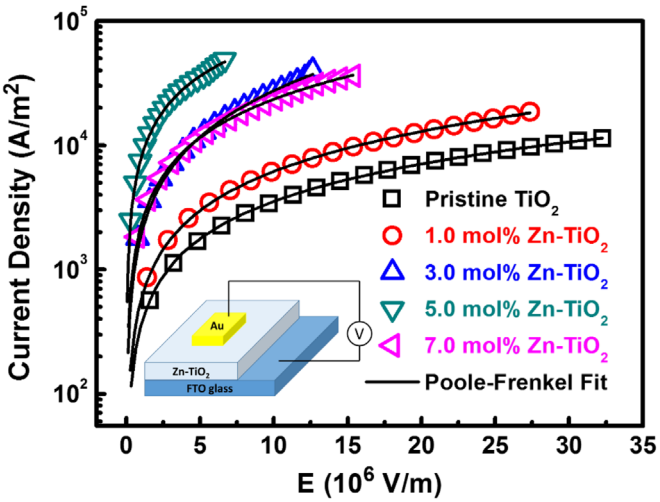

Fig. 3. The current density-electric field (J-E) curves of the various Zn-doped TiO_2 compact layers and the inset is the schematic diagram of testing structure.

Table 1
Summary of conductivity of various Zn-doped TiO_2 compact layers.

Sample name	Conductivity (mS/m)
Pristine TiO_2	0.35
1.0 mol% Zn-doped TiO_2	0.55
3.0 mol% Zn-doped TiO_2	1.57
5.0 mol% Zn-doped TiO_2	8.34
7.0 mol% Zn-doped TiO_2	2.20

Fig. 4(a-d). However, some sub-micron scale concave domains are formed on the surface of Zn-doped TiO_2 compact layer when doping concentration is 7.0 mol% (Fig. 4(e)). AFM was adopted to measure the surface roughness of various Zn-doped TiO_2 compact layers. AFM images of various Zn-doped TiO_2 compact layers are shown in Fig. S1 of Supporting information. The root mean square (RMS) of roughness is a function that takes the square of the measured values. Moreover, the RMS roughness analysis for Zn-doped TiO_2 compact layer indicated that the RMS roughness increased from 18.88 to 23.03 nm with increasing the Zn doping concentration from 0.0 to 7.0 mol% (Fig. 4(f)). The RMS roughness of 7.0 mol% Zn-doped TiO_2 compact layer shows the apparent void formation. Shen et al. reported that Zn-doped TiO_2 (~8.0 mol%) cause the defect microstructures due to oxygen deficiency and minor Zn_2TiO_4 phases formation on rutile TiO_2 surface [40,41]. The surface roughness of Zn-doped TiO_2 compact layer played a crucial role in determining the electron transport behavior. It affected the interface area between perovskite active layer (i.e., $CH_3NH_3PbI_{3-x}Cl_x$) and Zn-doped TiO_2 compact layer.

The photoinduced charge carrier dynamics are investigated in detail using TRPL spectra. We measured static PL (Fig. 5(a)) and transient PL decay (Fig. 5(b)) of samples consisted of $CH_3NH_3PbI_{3-x}Cl_x$ /Zn-doped TiO_2. The PL intensity decreases with Zn doping concentration from 0.0 to 5.0 mol%. The 5.0 mol% Zn-doped TiO_2 sample shows the highest PL quenching resulted from its highest conductivity for fast charge transport. To further check the charge transfer rate and the charge separation efficiency, the transient PL decay plots of the various Zn-doped TiO_2 sample were measured by time-correlated single photon counting (TCSPC). The transient PL decay plots were fitted by tri-exponential decay kinetics function:

$$F(t)=A_1\exp\left(-\frac{t}{\tau_1}\right)+A_2\exp\left(-\frac{t}{\tau_2}\right)+A_3\exp\left(-\frac{t}{\tau_3}\right)$$

where A_1, A_2 and A_3 are time independent coefficient of amplitude fraction, respectively. τ_1, τ_2 and τ_3 are fast decay time, intermediate decay time and slow decay time. The average decay time was calculated using the following equation:

$$\tau_{avg}=\sum_i A_i\tau_i/\sum_i A_i$$

The transient PL decay fitting curve of $CH_3NH_3PbI_{3-x}Cl_x$/Zn-doped TiO_2 depicts the Zn doping could influence the charge transport efficiency. Table S1 is the summary of measured fast decay time (τ_1), intermediate decay time (τ_2), slow decay time (τ_3), and PL average lifetime (τ_{avg}) for $CH_3NH_3PbI_{3-x}Cl_x$/Zn-doped TiO_2. The 5.0 mol% Zn-doped TiO_2 sample shows the shortest PL average lifetime of 8.9 ns, it consists with the highest quenching effect shown in Fig. 5(a). Thus, the 5.0 mol% Zn-doped TiO_2 compact layer exhibits highest charge separation rate. These results may be attributed to the high charge carrier transport of Zn-doped TiO_2.

The various Zn-doped TiO_2 compact layers were used as the electron transport layers of perovskite solar cells. The configuration of our perovskite solar cell is FTO/Zn-doped TiO_2/$CH_3NH_3PbI_{3-x}Cl_x$ /Spiro-OMeTAD/Au electrode, as shown in Fig. 6(a). The J-V curves and performance of different perovskite solar cells fabricated by various Zn-doped TiO_2 compact layers are shown in Fig. 6(b) and Table 2, respectively. The open-circuit voltage (V_{oc}) is decreased from 0.95 to 0.90 V with increasing Zn doping concentration from 0.0 to 7.0 mol% as the result of the lower Zn-doped TiO_2 conduction band. The lower conduction band of Zn-doped TiO_2 facilitates electron injection and electron transport compared with pristine TiO_2. Many literatures also reported that electron can be transferred easily from TiO_2 to ZnO due to the electron affinity and the band alignment [42–44]. The J_{sc} is increased from 18.5 to 22.3 mA/cm^2 with increasing Zn-doping concentration from 0.0 to 5.0 mol% due to the increased electrical conductivity and improved charge transport. The perovskite solar cell with 7.0 mol% Zn-doped TiO_2 compact layer exhibits reduced J_{sc} of 18.5 mA/cm^2. We suggest that the reduced J_{sc} at 7.0 mol% Zn-doped TiO_2 device is caused by the formation of voids. For the fill factors (FF) of fabricated perovskite solar cells, the values are similar and lies between 64.7% and 68.8%. The PCE of the perovskite solar cell with pristine TiO_2 compact layer is 11.3%. When increasing Zn doping concentrations from 1.0 to 5.0 mol%, the PCE is improved from 11.8 to 14.0%. For 7.0 mol% Zn dopant, its PCE is decreased to 11.1% compare to pristine TiO_2 compact layer (Fig. 6(c)). Hence, the PCE performance is correlated to the morphology of TiO_2 compact layer and the efficiency of charge transport and charge separation. The average performance of the perovskite solar cell with Zn-doped TiO_2 compact layer was dominated by J_{sc}. After optimizing the processing parameters of perovskite solar cells, a maximum efficiency was attained for the cell fabricated from 5.0 mol% Zn-doped TiO_2, with $J_{sc}=22.3\pm0.3$ mA/cm^2, $V_{oc}=0.91\pm0.01$ V, FF $=68.8\pm3.7\%$ and PCE $=14.0\pm1.5\%$, respectively. The EQE spectra of the perovskite solar cells with different Zn-doped TiO_2 compact layers (Fig. 6(d)) confirm the improvement of charge separation efficiency by Zn doping. The J_{sc} of 5.0 mol% Zn-doped TiO_2 device estimated from the EQE spectrum is ~17.1 mA/cm^2, lower than the average J_{sc} (~22.3 mA/cm^2). The reason implies the anomalous hysteresis for the planar perovskite solar cells [45]. For the hysteresis measurement, Fig. S2 and Table S2 show the characteristics of pristine TiO_2 and 5.0 mol% Zn-doped TiO_2 device scan in reverse and forward directions. The PCE of pristine TiO_2 device with forward bias is 8.9% lower than that 10.6% with reverse bias. The PCE of 5.0 mol% Zn-doped TiO_2 device with forward bias is 11.2% while the reverse bias is 13.8%. The hysteresis phenomenon would be the unbalance of the electron and hole flux in the planar n-i-p perovskite solar cells [6,26,46–48].

The chemical compositions of various Zn-doped TiO_2 compact layers were investigated by XPS. The peak position of Ti $2p_{3/2}$ binding energy in various Zn-doped TiO_2 compact layer is at

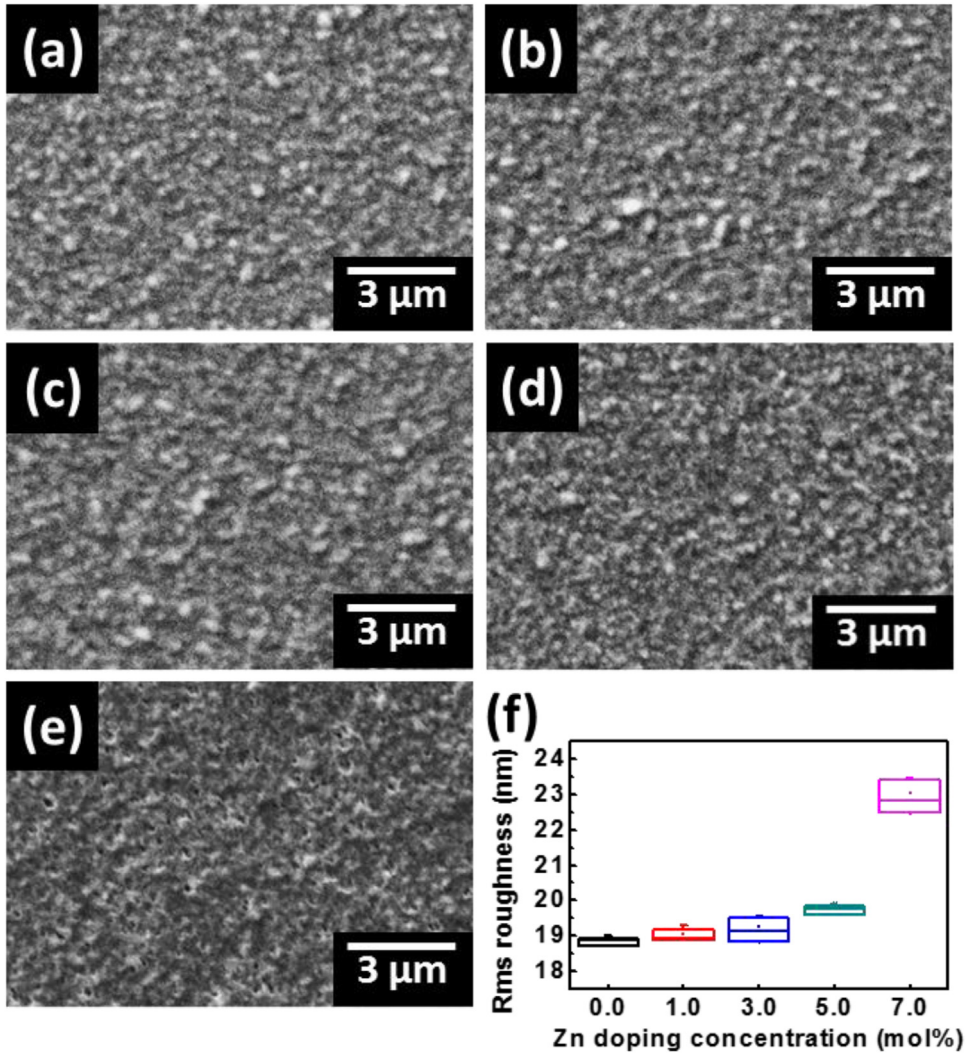

Fig. 4. SEM images of (a) pristine TiO_2 compact layer and various Zn-doped TiO_2 compact layers, including (b) 1.0 mol% Zn-TiO_2, (c) 3.0 mol% Zn-TiO_2, (d) 5.0 mol% Zn-TiO_2, and (e) 7.0 mol% Zn-TiO_2. (f) The RMS roughness distribution of various Zn-doped TiO_2 compact layers are measured by AFM.

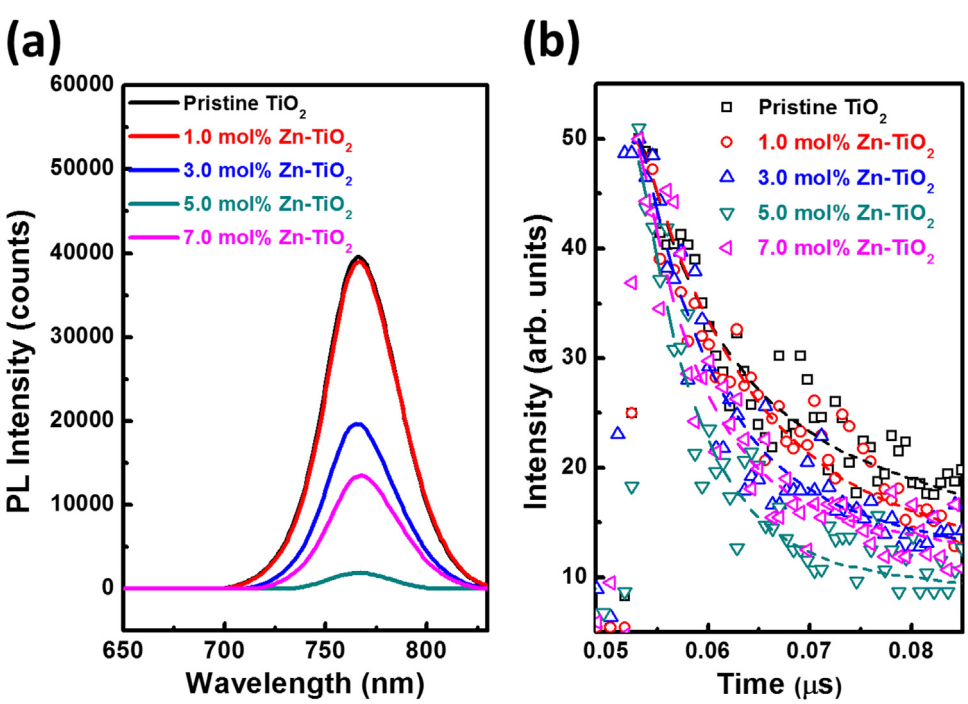

Fig. 5. Photoluminescence spectra using (a) static and (b) time-resolved of $CH_3NH_3PbI_{3-x}Cl_x$/Zn-doped TiO_2/FTO measured at room temperature.

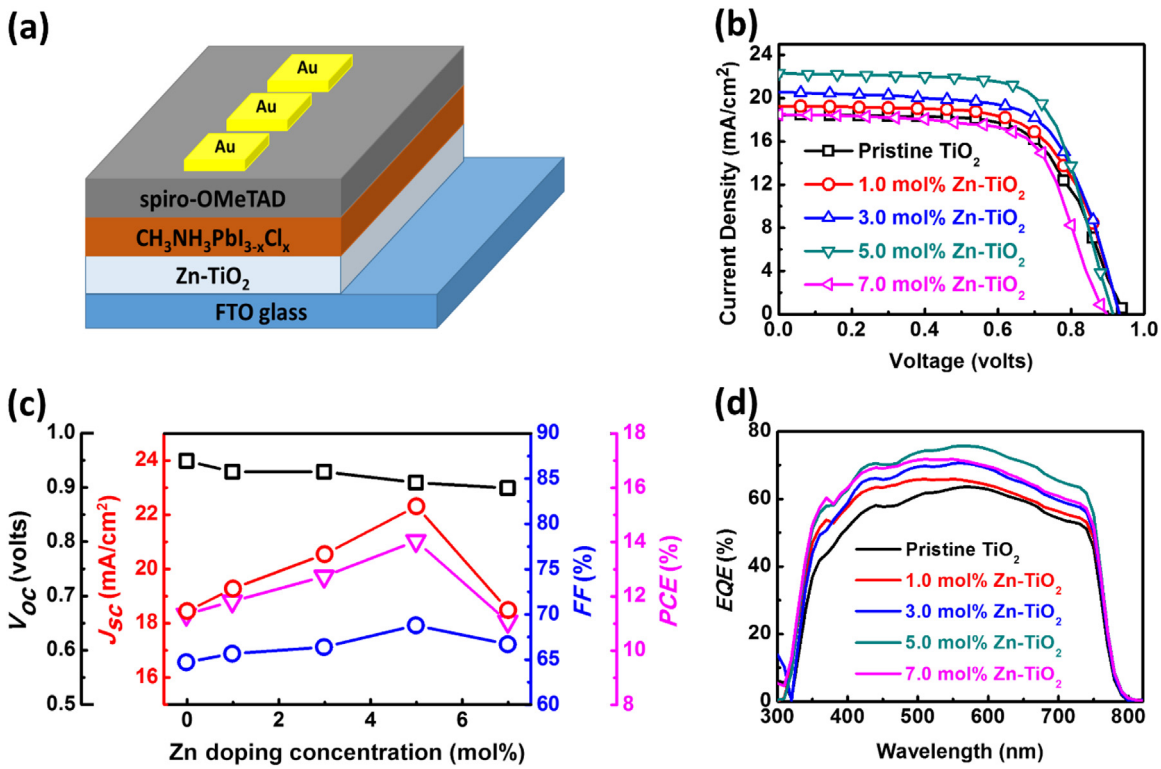

Fig. 6. (a) The schematic diagram of perovskite solar cell structure. (b) J-V curves, (c) the plots of photovoltaic characteristics, and (d) EQE spectra of the perovskite solar cells with different Zn-doped TiO_2 compact layer.

Table 2
Characteristics of perovskite solar cells with different Zn doping concentration in the TiO_2 compact layer.

Sample name	V_{oc} (V)	J_{sc} (mA/cm^2)	*FF* (%)	η (%)
Pristine TiO_2	0.95 ± 0.01	18.5 ± 0.6	64.7 ± 2.6	11.3 ± 1.1
1.0 mol% Zn-doped TiO_2	0.93 ± 0.02	19.3 ± 0.5	65.7 ± 3.4	11.8 ± 1.0
3.0 mol% Zn-doped TiO_2	0.93 ± 0.01	20.6 ± 0.9	66.4 ± 3.0	12.7 ± 1.5
5.0 mol% Zn-doped TiO_2	0.91 ± 0.01	22.3 ± 0.3	68.8 ± 3.6	14.0 ± 1.5
7.0 mol% Zn-doped TiO_2	0.90 ± 0.02	18.5 ± 0.7	66.7 ± 2.2	11.1 ± 1.7

Table 3
The theoretical and experimental atomic ratios of Zn/Zn+Ti in pristine TiO_2 and various Zn-doped TiO_2.

Sample name	Zn/Zn+Ti (%)	
	Theoretical value	XPS analysis
Pristine TiO_2	0.0	0.0
1.0 mol% Zn-doped TiO_2	1.0	1.5
3.0 mol% Zn-doped TiO_2	3.0	4.5
5.0 mol% Zn-doped TiO_2	5.0	6.2
7.0 mol% Zn-doped TiO_2	7.0	8.6

458.5 eV [49]. For Zn XPS spectra, the two peak positions at 1022 eV and 1044 eV are corresponding to Zn $2p_{3/2}$ and Zn $2p_{1/2}$ [27]. After analyzing the XPS data, the atomic ratios of Zn/Zn+Ti for various Zn-doped TiO_2 compact layers are shown in Table 3. We also prepared the 5.0 mol% Zn-doped TiO_2 film (~700 nm) for SEM/EDS analysis, and field emission-SEM images of this film are shown in Fig. S3(a, b). It exhibits many significantly cracks on this film compared with Zn-doped TiO_2 thin film (~90 nm, the compact layer used in the perovskite solar cells) [50,51]. Then we measured EDS spectra and chemical compositions of selected 6 point positions as shown in Fig. S3(c) and Table S3. The EDS result shows that the Zn element are homogenously distributed within Zn-doped TiO_2 film.

4. Conclusion

In summary, various Zn-doped TiO_2 compact layers with different concentrations of Zn doping are prepared successfully by sol-gel method followed by thermal treatment. The effects of Zn doping concentration on the changes of optical absorption behavior, electrical conductivity, surface morphology and charge carrier dynamics are systemically studied. For Zn doping concentration less than 5.0 mol%, the absorption behavior, electrical conductivity and charge separation efficiency increase with Zn doping concentration. However, the large amount Zn doping (>7.0 mol%) results in the decay of these properties due to formation of voids. After optimizing the processing parameters of perovskite solar cells, the J_{sc} is increased from 18.5 to 22.3 mA/cm^2 and the PCE is improved from 11.3 to 14.0% by using 5.0 mol% Zn-doped TiO_2 compact layer.

Acknowledgment

The authors appreciate Dr. Ming-Tao Lee group (BL-13A1) at National Synchrotron Radiation Research Center and Dr. Tz-Feng Lin at Chang Gung University for useful discussion and suggestions. The authors acknowledge the financial support from Ministry of Science and Technology of Taiwan (MOST 103-2221-E-182-008-MY2, MOST 105-2632-E-182-001, and MOST 105-3113-E-002-010), Chang Gung University Research Project (UERPD2D0041), and Chang Gung Memorial Hospital, Linkou, Taiwan (CMRPD2E0071 and BMRPD074).

Appendix A. Supplementary material

Supplementary data associated with this article can be found in the online version at http://dx.doi.org/10.1016/j.solmat.2016.07.003.

References

[1] ⟨http://www.nrel.gov/ncpv/images/efficiency_chart.jpg⟩.
[2] N. Espinosa, L. Serrano-Luján, A. Urbina, F.C. Krebs, Solution and vapour deposited lead perovskite solar cells: ecotoxicity from a life cycle assessment perspective, Sol. Energy Mater. Sol. Cells 137 (2015) 303–310.
[3] C.-G. Wu, C.-H. Chiang, Z.-L. Tseng, M.K. Nazeeruddin, A. Hagfeldt, M. Gratzel, High efficiency stable inverted perovskite solar cells without current hysteresis, Energy Environ. Sci. 8 (2015) 2725–2733.
[4] M. Liu, M.B. Johnston, H.J. Snaith, Efficient planar heterojunction perovskite solar cells by vapour deposition, Nature 501 (2013) 395–398.
[5] N.J. Jeon, J.H. Noh, W.S. Yang, Y.C. Kim, S. Ryu, J. Seo, S.I. Seok, Compositional engineering of perovskite materials for high-performance solar cells, Nature 517 (2015) 476–480.
[6] N.J. Jeon, J.H. Noh, Y.C. Kim, W.S. Yang, S. Ryu, S.I. Seok, Solvent engineering for high-performance inorganic–organic hybrid perovskite solar cells, Nat. Mater. 13 (2014) 897–903.
[7] J.P. Correa Baena, L. Steier, W. Tress, M. Saliba, S. Neutzner, T. Matsui, F. Giordano, T.J. Jacobsson, A.R. Srimath Kandada, S.M. Zakeeruddin, A. Petrozza, A. Abate, M.K. Nazeeruddin, M. Gratzel, A. Hagfeldt, Highly efficient planar perovskite solar cells through band alignment engineering, Energy Environ. Sci. 8 (2015) 2928–2934.
[8] Y. Yamada, T. Nakamura, M. Endo, A. Wakamiya, Y. Kanemitsu, Photocarrier Recombination Dynamics in Perovskite $CH_3NH_3PbI_3$ for Solar Cell Applications, J. Am. Chem. Soc. 136 (2014) 11610–11613.
[9] N. Marinova, W. Tress, R. Humphry-Baker, M.I. Dar, V. Bojinov, S. M. Zakeeruddin, M.K. Nazeeruddin, M. Grätzel, Light harvesting and charge recombination in $CH_3NH_3PbI_3$ perovskite solar cells studied by hole transport layer thickness variation, ACS Nano 9 (2015) 4200–4209.
[10] G.S. Han, H.S. Chung, B.J. Kim, D.H. Kim, J.W. Lee, B.S. Swain, K. Mahmood, J. S. Yoo, N.-G. Park, J.H. Lee, H.S. Jung, Retarding charge recombination in perovskite solar cells using ultrathin MgO-coated TiO_2 nanoparticulate films, J. Mater. Chem. A 3 (2015) 9160–9164.
[11] M.M. Lee, J. Teuscher, T. Miyasaka, T.N. Murakami, H.J. Snaith, Efficient hybrid solar cells based on meso-superstructured organometal halide perovskites, Science 338 (2012) 643–647.
[12] D.-Y. Son, J.-H. Im, H.-S. Kim, N.-G. Park, 11% efficient perovskite solar cell based on ZnO nanorods: an effective charge collection system, J. Phys. Chem. C 118 (2014) 16567–16573.
[13] D. Bi, S.-J. Moon, L. Haggman, G. Boschloo, L. Yang, E.M.J. Johansson, M. K. Nazeeruddin, M. Gratzel, A. Hagfeldt, Using a two-step deposition technique to prepare perovskite ($CH_3NH_3PbI_3$) for thin film solar cells based on ZrO_2 and TiO_2 mesostructures, RSC Adv. 3 (2013) 18762–18766.
[14] X. Wang, Z. Li, W. Xu, S.A. Kulkarni, S.K. Batabyal, S. Zhang, A. Cao, L.H. Wong, TiO_2 nanotube arrays based flexible perovskite solar cells with transparent carbon nanotube electrode, Nano Energy 11 (2015) 728–735.
[15] T.-S. Su, T.-Y. Hsieh, C.-Y. Hong, T.-C. Wei, Electrodeposited ultrathin TiO_2 blocking layers for efficient perovskite solar cells, Sci. Rep. 5 (2015) 16098.
[16] G. Murugadoss, G. Mizuta, S. Tanaka, H. Nishino, T. Umeyama, H. Imahori, S. Ito, Double functions of porous TiO_2 electrodes on $CH_3NH_3PbI_3$ perovskite solar cells: enhancement of perovskite crystal transformation and prohibition of short circuiting, APL Mater. 2 (2014) 081511.
[17] R. Lindblad, D. Bi, B.-w Park, J. Oscarsson, M. Gorgoi, H. Siegbahn, M. Odelius, E. M.J. Johansson, H. Rensmo, , Electronic structure of $TiO_2/CH_3NH_3PbI_3$ perovskite solar cell interfaces, J. Phys. Chem. Lett. 5 (2014) 648–653.
[18] W. Ke, G. Fang, J. Wang, P. Qin, H. Tao, H. Lei, Q. Liu, X. Dai, X. Zhao, Perovskite solar cell with an efficient TiO_2 compact film, ACS Appl. Mater. Interfaces 6 (2014) 15959–15965.
[19] T. Zhu, S.-P. Gao, The stability, electronic structure, and optical property of TiO_2 polymorphs, J. Phys. Chem. C 118 (2014) 11385–11396.
[20] H. Yu, S. Zhang, H. Zhao, G. Will, P. Liu, An efficient and low-cost TiO_2 compact layer for performance improvement of dye-sensitized solar cells, Electrochim. Acta 54 (2009) 1319–1324.
[21] J. van de Lagemaat, N.G. Park, A.J. Frank, Influence of electrical potential distribution, charge transport, and recombination on the photopotential and photocurrent conversion efficiency of dye-sensitized nanocrystalline TiO_2 solar cells: a study by electrical impedance and optical modulation techniques, J. Phys. Chem. B 104 (2000) 2044–2052.
[22] G.S. Han, Y.H. Song, Y.U. Jin, J.-W. Lee, N.-G. Park, B.K. Kang, J.-K. Lee, I.S. Cho, D. H. Yoon, H.S. Jung, Reduced graphene oxide/mesoporous TiO_2 nanocomposite based perovskite solar cells, ACS Appl. Mater. Interfaces 7 (2015) 23521–23526.
[23] M. Yang, R. Guo, K. Kadel, Y. Liu, K. O'Shea, R. Bone, X. Wang, J. He, W. Li, Improved charge transport of Nb-doped TiO_2 nanorods in methylammonium lead iodide bromide perovskite solar cells, J. Mater. Chem. A 2 (2014) 19616–19622.
[24] H. Zhou, Q. Chen, G. Li, S. Luo, T.-b Song, H.-S. Duan, Z. Hong, J. You, Y. Liu, Y. Yang, Interface engineering of highly efficient perovskite solar cells, Science 345 (2014) 542–546.
[25] J. Wang, M. Qin, H. Tao, W. Ke, Z. Chen, J. Wan, P. Qin, L. Xiong, H. Lei, H. Yu, G. Fang, Performance enhancement of perovskite solar cells with Mg-doped TiO_2 compact film as the hole-blocking layer, Appl. Phys. Lett. 106 (2015) 121104.
[26] J.H. Heo, M.S. You, M.H. Chang, W. Yin, T.K. Ahn, S.-J. Lee, S.-J. Sung, D.H. Kim, S. H. Im, Hysteresis-less mesoscopic $CH_3NH_3PbI_3$ perovskite hybrid solar cells by introduction of Li-treated TiO_2 electrode, Nano Energy 15 (2015) 530–539.
[27] A.H. Ghanbari Niaki, A.M. Bakhshayesh, M.R. Mohammadi, Double-layer dye-sensitized solar cells based on Zn-doped TiO_2 transparent and light scattering layers: improving electron injection and light scattering effect, Sol. Energy 103 (2014) 210–222.
[28] K.-P. Wang, H. Teng, Zinc-doping in TiO_2 films to enhance electron transport in dye-sensitized solar cells under low-intensity illumination, Phys. Chem. Chem. Phys. 11 (2009) 9489–9496.
[29] F. Zhu, P. Zhang, X. Wu, L. Fu, J. Zhang, D. Xu, The Origin of higher open-circuit voltage in Zn-doped TiO_2 nanoparticle-based dye-sensitized solar cells, ChemPhysChem 13 (2012) 3731–3737.
[30] A. Vlasa, S. Varvara, A. Pop, C. Bulea, L. Muresan, Electrodeposited Zn–TiO_2 nanocomposite coatings and their corrosion behavior, J. Appl. Electrochem. 40 (2010) 1519–1527.
[31] H.-H. Wang, Q. Chen, H. Zhou, L. Song, Z.S. Louis, N.D. Marco, Y. Fang, P. Sun, T.-B. Song, H. Chen, Y. Yang, Improving the TiO_2 electron transport layer in perovskite solar cells using acetylacetonate-based additives, J. Mater. Chem. A 3 (2015) 9108–9115.
[32] H.-S. Kim, C.-R. Lee, J.-H. Im, K.-B. Lee, T. Moehl, A. Marchioro, S.-J. Moon, R. Humphry-Baker, J.-H. Yum, J.E. Moser, M. Grätzel, N.-G. Park, Lead iodide perovskite sensitized all-solid-state submicron thin film mesoscopic solar cell with efficiency exceeding 9%, Sci. Rep. 2 (2012) 591.
[33] C.-Y. Chang, C.-Y. Chu, Y.-C. Huang, C.-W. Huang, S.-Y. Chang, C.-A. Chen, C.-Y. Chao, W.-F. Su, Tuning perovskite morphology by polymer additive for high efficiency solar cell, ACS Appl. Mater. Interfaces, 7, (2015) 4955–4961.
[34] D. Liu, T.L. Kelly, Perovskite solar cells with a planar heterojunction structure prepared using room-temperature solution processing techniques, Nat. Photonics 8 (2014) 133–138.
[35] H.J. Snaith, A. Abate, J.M. Ball, G.E. Eperon, T. Leijtens, N.K. Noel, S.D. Stranks, J. T.-W. Wang, K. Wojciechowski, W. Zhang, Anomalous hysteresis in perovskite solar cells, J. Phys. Chem. Lett. 5 (2014) 1511–1515.
[36] M. Thambidurai, J.Y. Kim, Y. Ko, H.-j Song, H. Shin, J. Song, Y. Lee, N. Muthukumarasamy, D. Velauthapillai, C. Lee, High-efficiency inverted organic solar cells with polyethylene oxide-modified Zn-doped TiO_2 as an interfacial electron transport layer, Nanoscale 6 (2014) 8585–8589.
[37] Z. Fu, J. Zhang, X. Yang, W. Cao, Preparation of nano-crystal N-Zn/TiO_2 anode films and the effects of co-sensitization on the performance of dye-sensitized solar cells, Chin. Sci. Bull. 56 (2011) 2001–2008.
[38] D.O. Scanlon, C.W. Dunnill, J. Buckeridge, S.A. Shevlin, A.J. Logsdail, S. M. Woodley, C.R.A. Catlow, M.J. Powell, R.G. Palgrave, I.P. Parkin, G.W. Watson, T.W. Keal, P. Sherwood, A. Walsh, A.A. Sokol, Band alignment of rutile and anatase TiO_2, Nat. Mater. 12 (2013) 798–801.
[39] S.M. Yoon, S.J. Lou, S. Loser, J. Smith, L.X. Chen, A. Facchetti, T. Marks, Fluorinated copper phthalocyanine nanowires for enhancing interfacial electron transport in organic solar cells, Nano Lett. 12 (2012) 6315–6321.
[40] T.-j Chen, P. Shen, Defect clustering and ordering in Zn-doped TiO_2 upon solution annealing, J. Phys. Chem. C 113 (2009) 328–332.
[41] G.M. Zeer, E.G. Zelenkova, N.S. Nikolaeva, S.M. Zharkov, S.I. Pochekutov, O. N. Ledyaeva, A.B. Sartpaeva, A.A. Mikheev, Formation of phases and microstructure of ZnO and TiO_2 based ceramic, Glass Ceram. 72 (2015) 242–245.
[42] S. Chen, J.R. Manders, S.-W. Tsang, F. So, Metal oxides for interface engineering in polymer solar cells, J. Mater. Chem. 22 (2012) 24202–24212.
[43] R. Wang, H. Tan, Z. Zhao, G. Zhang, L. Song, W. Dong, Z. Sun, Stable ZnO@TiO_2 core/shell nanorod arrays with exposed high energy facets for self-cleaning coatings with anti-reflective properties, J. Mater. Chem. A 2 (2014) 7313–7318.
[44] J. Tian, Q. Zhang, E. Uchaker, R. Gao, X. Qu, S. Zhang, G. Cao, Architectured ZnO photoelectrode for high efficiency quantum dot sensitized solar cells, Energy Environ. Sci. 6 (2013) 3542–3547.
[45] F. Wang, H. Yu, H. Xu, N. Zhao, HPbI3: a new precursor compound for highly efficient solution-processed perovskite solar cells, Adv. Funct. Mater. 25 (2015) 1120–1126.
[46] Y. Liyan, T.B. Alexander, G.L. David, W. Tao, Recent progress and challenges of organometal halide perovskite solar cells, Rep. Prog. Phys. 79 (2016) 026501.
[47] H.-S. Kim, N.-G. Park, Parameters affecting I–V hysteresis of $CH_3NH_3PbI_3$ perovskite solar cells: effects of perovskite crystal size and mesoporous TiO_2 layer, J. Phys. Chem. Lett. 5 (2014) 2927–2934.
[48] S.D. Sung, D.P. Ojha, J.S. You, J. Lee, J. Kim, W.I. Lee, 50 nm sized spherical TiO_2 nanocrystals for highly efficient mesoscopic perovskite solar cells, Nanoscale 7 (2015) 8898–8906.
[49] M.-C. Wu, J. Hiltunen, A. Sápi, A. Avila, W. Larsson, H.-C. Liao, M. Huuhtanen, G. Tóth, A. Shchukarev, N. Laufer, Á. Kukovecz, Z. Kónya, J.-P. Mikkola, R. Keiski, W.-F. Su, Y.-F. Chen, H. Jantunen, P.M. Ajayan, R. Vajtai, K. Kordás, Nitrogen-doped anatase nanofibers decorated with noble metal nanoparticles for photocatalytic production of hydrogen, ACS Nano 5 (2011) 5025–5030.
[50] Á.A. Ramírez-Santos, P. Acevedo-Peña, E.M. Córdoba, Photo-assisted electrochemical copper removal from cyanide solutions using porous TiO_2 thin film photo-anodes, Mat. Res. 17 (2014) 69–77.
[51] M. Bockmeyer, P. Löbmann, Crack formation in TiO_2 films prepared by sol–gel processing: quantification and characterization, Thin Solid Films 515 (2007) 5212–5219.

Please cite this article as: M.-C. Wu, et al., Enhanced short-circuit current density of perovskite solar cells using Zn-doped TiO_2 as electron transport layer, Solar Energy Materials and Solar Cells (2016), http://dx.doi.org/10.1016/j.solmat.2016.07.003